UNCERTAINTY AND SENSITIVITY ANALYSIS OF COBRA-TF FOR THE OECD LWR UAM BENCHMARK USING DAKOTA

N. Porter, M. Avramova, K. Ivanov
Pennsylvania State University
231 Reber Building, University Park, PA 16802, USA
nwp110@psu.edu; mna109@psu.edu; kni@psu.edu

ABSTRACT

This paper describes the results of a quantitative statistical uncertainty analysis of five cases from the OECD/NEA Uncertainty Analysis in Modeling (UAM) Benchmark. The codes used for this study were the Pennsylvania State University (PSU) version of the thermal hydraulic subchannel code COBRA-TF (COolant Boiling in Rod Array – Two Fluid) and the statistical analysis tool Dakota (Design Analysis Kit for Optimization and Terascale Applications) from Sandia National Laboratories. Four steady state cases and one transient case are included from Phase II, Exercise 3 of the UAM Benchmark.

A large variety of output parameters are analyzed for each test case: maximum void fraction, maximum fuel temperature, maximum cladding temperature, bundle pressure drop, a variety of axial distributions for a central subchannel, and the radial distribution of void fraction at the exit of the assembly. The predicted uncertainty in all parameters is low for all cases. The dominant sources of uncertainty are inferred from rank correlation coefficients between the input and output parameters.

The results agree well with similar past studies, but using a different method for sample size selection and the newest versions of the UAM benchmark and COBRA-TF. This study makes the following contributions to the existing literature: an analysis of the axial development of sensitivity information, the inclusion of a transient case, and an in-depth analysis of the geometry uncertainty treatment suggested by the UAM benchmark. Recommendations for future work are made, with an emphasis on the importance of a quantitative method for determination of the modeling parameter uncertainties.

KEYWORDS
Thermal hydraulics, uncertainty analysis, subchannel codes, COBRA-TF, Dakota

1. INTRODUCTION

In the nuclear community, traditional conservative analyses are increasingly being replaced by best-estimate calculations with uncertainty quantification. To aid in this transition, the OECD/NEA Nuclear Science Committee Expert Group on Uncertainty Analysis in Modeling is developing the UAM Benchmark [1] to assess uncertainty in reactor physics, fuel performance, thermal hydraulics, and coupled multi-physics calculations. Phase II, Exercise 3 of the UAM benchmark provides twelve test cases that focus on the uncertainty in nuclear thermal hydraulic codes. These test cases are divided equally among three common types of light water reactors (LWRs): PWR, BWR, and VVER.

A comprehensive statistical uncertainty analysis was performed on COBRA-TF in order to better understand the sources and behavior of uncertainties. This paper describes the computational methods used, outlines the UAM specification, reports results and offers a concluding discussion.

2. COMPUTATIONAL TOOLS

The uncertainty of the PSU Reactor Dynamics and Fuel Management Group (RDFMG) version of the subchannel code COBRA-TF (CTF) [2], which is developed in conjunction with the Consortium for the Simulation of LWRs (CASL), is used. The statistical analysis tool Dakota [3] is used to automate much of the repetitive processes necessary for a statistical uncertainty analysis.

2.1. COBRA-TF: Thermal Hydraulic Subchannel Code

COBRA-TF is a thermal hydraulic subchannel code designed for the analysis of rod bundles inside a nuclear core. The code was originally developed as part of COBRA/TRAC at Pacific Northwest National Laboratory in 1980. Various versions of COBRA-TF have been created throughout academia and industry over the last few decades. One of these versions, rebranded as "CTF", has been improved and developed by the RDFMG at PSU since the 1990's. CTF has recently been incorporated into the CASL project, which has led to rapid improvements in the modeling capabilities, parallelization, performance, documentation, and validation of the code [4].

The CASL version of CTF uses a two fluid, three field representation of two-phase flow. A total of eight conservation equations are solved for the fluid region: the mass, momentum and energy equations for the continuous liquid and vapor, as well as mass and momentum equations for the entrained liquid droplets.

The code can model both normal operating conditions and accident scenarios, and it includes models for a wide range of thermal hydraulic phenomena that are important to nuclear reactor analysis. CTF realistically represents fuel assemblies using models of physical structures such as nuclear fuel rods, heated conductors, unheated conductors and spacer grids. All of these features, and others that have not been mentioned, make the code extremely versatile and well-suited for various applications in both academia and industry.

2.2. Dakota: Statistical Analysis Tool

Dakota is a statistical analysis tool that provides an extensive interface between simulation codes and iterative analysis methods. It is developed at Sandia National Laboratories and includes a variety of tools to aid in uncertainty and sensitivity analysis, code validation and verification, as well as calibration and creation of surrogate models. Dakota is the recommended software for Validation and Uncertainty Quantification (VUQ) work within the CASL program [5], so it was the natural choice for this study.

The method used for this study was an incremental uncertainty analysis with statistical sampling. Dakota performs each of the following tasks iteratively until the desired sample size is reached:

1. Simultaneously sample from each of the input parameter distributions.
2. Execute the pre-processing script, which uses a template CTF input deck and the input parameters from the first step to create the input deck for the current run.
3. Run CTF.
4. Execute the post-processing script, which extracts all output parameters from the CTF output files.

This process is illustrated in Figure 1; the center loop shows the execution of scripts, while the outer loop demonstrates the actual processes taking place. When the desired sample size is reached, Dakota automatically calculates statistical parameters: the mean, standard deviation, skew, and kurtosis of each of the output parameters. In addition, Spearman rank correlation coefficients (RCCs) between the inputs and outputs are also calculated. For this study, RCCs measure the linear relationship between two parameters.

An RCC of +1 indicates a perfectly linear relationship between two parameters; as the input increases, so does the output. If the RCC is -1, the relationship is linear, but as one increases, the other will decrease. If there is no relationship between the two parameters, the RCC is zero.

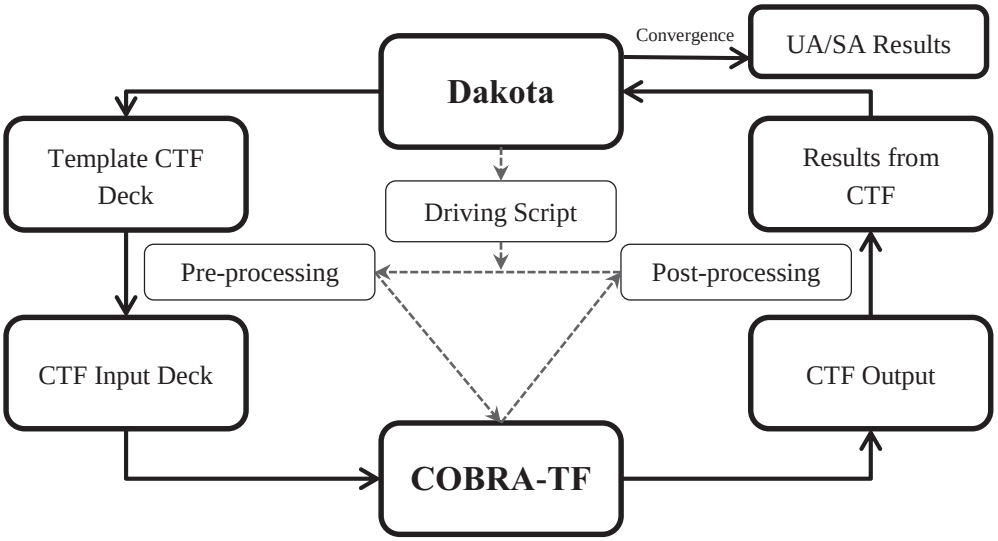

Figure 1. CTF/Dakota external coupling scheme

For this study, the desired sample size was determined directly from the convergence of the statistical parameters, rather than using a criterion such as Wilk's Formula [6]. The sample size was incrementally increased until all statistical parameters (mean, standard deviation, and RCCs for each output parameter) were converged to a set tolerance. The statistical parameters are calculated for the n^{th} iteration, and these are compared to their values for the *n-1* iteration using Equation 1, where ε is the percent difference and x is any given statistical parameter.

$$\varepsilon = 100 * \left(\frac{x_{n-1} - x_n}{x_{n-1}}\right) \quad (1)$$

If any of the statistical parameters differ by more than 1%, a new iteration is computed (*n+1*) and the process is continued. This method was implemented using an external script that assesses the convergence of all output parameters, where each iteration increases the sample size by five CTF runs. The use of this method ensures that the sample size is large enough for statistically significant results, while also conserving computational resources.

3. UAM SPECIFICATIONS

The benchmark specifies all parameters necessary to model each case. All uncertainties are simultaneously propagated through CTF to find their effects on the output parameters. The outputs requested by the UAM benchmark are as follows: the global maximum of the void fraction, outside cladding temperature, and fuel or rod centerline temperature; axial distributions in a central channel/rod of the: void fraction, cladding outside temperature, fuel or rod centerline temperature; and a radial distribution of the void fraction at the exit of the assembly. This section will briefly describe the geometry and boundary conditions for each of the steady state cases and the transient case, and will describe the input uncertainties propagated in this study. More information can be found in the benchmark itself [1].

3.1. Steady State Cases

The uncertainty of CTF was quantified for four steady state cases from Exercise II-3 of the UAM benchmark: 1a, 2a, 4a, and 5a. An axial cross-section of the geometry for each case is shown in Figure 2. For each case, the grey rod and channel indicate the locations from which axial distributions are taken. The boundary conditions for each of the four steady state cases are shown in Table I. Note that the parameters for Case 2a are for the quarter-assembly, not for the full assembly.

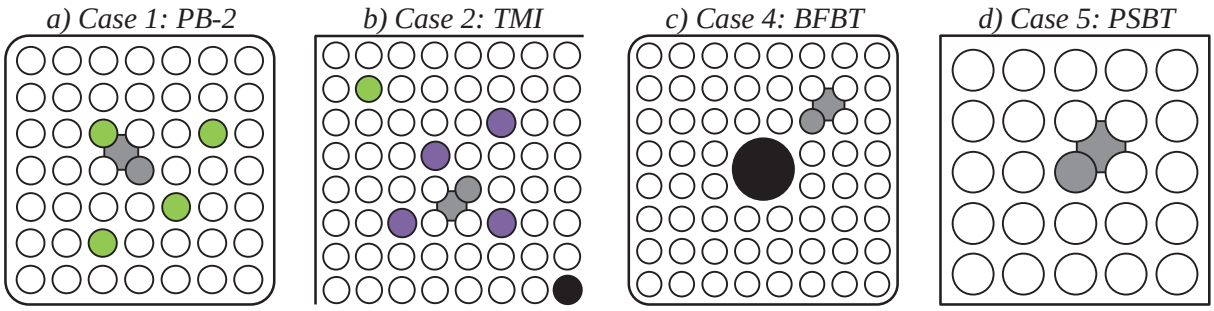

Figure 2. Geometry for all cases

Table I. Boundary conditions for the steady state cases

Assembly Parameter	Case 1a	Case 2a	Case 4a	Case 5a
Power (kWt)	4310	3915	3520	3376
Outlet Pressure (MPa)	7.0	15.2	7.16	16.43
Coolant Inlet Temperature (K)	543	565	551	580
Coolant flow rate (kg/s)	15.6	20.5	15.3	10.1

All CTF models for this work are coolant-centered. Case 1a models a 7x7 fuel bundle from the Peach Bottom Unit 2 (PB-2) plant. The rods highlighted in green contain gadolinium poison, and as such have a lower radial power. The CTF model of the assembly contains 30 axial nodes. A Three Mile Island Unit 1 (TMI-1) quarter-assembly is modeled for Case 2a. The green rod contains gadolinium poison, the purple rods indicate guide tube locations, and the black rod is the instrumentation tube at the center of the assembly. The TMI model has 30 axial nodes. This case is unique in the benchmark because there is very little void generation in the bundle. The third case, 4a, is Test 4101-58 from the OECD/NRC BFBT benchmark database [7]. It is similar to the PB-2 bundle, but it has a large water rod in the center, a uniform axial power profile, and has heated rods instead of nuclear fuel rods. The CTF model has 80 subchannels and 102 axial nodes of varying size. The final test is Case 5a, which is a 5x5 bundle from the OECD/NRC PSBT benchmark [8]. The CTF model of this case uses 55 axial nodes.

3.2. Transient Case

The transient cases in the UAM benchmark are very similar to the steady state cases, but the boundary conditions are varied over time. Results for one transient case, Case 2b, will be reported. This case models a five second flow reduction transient in the same assembly as Case 2a. The variation of the boundary conditions relative to the initial conditions is shown in Figure 3. The points used in the CTF deck are indicated by dots in the figure. CTF linearly interpolates between these points.

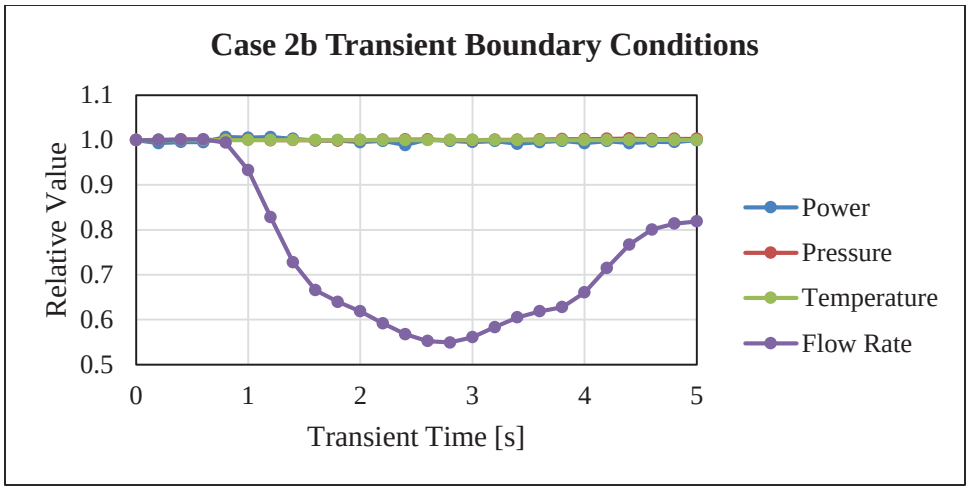

Figure 3. Case 2b transient boundary conditions

3.3. UAM Input Uncertainties

The input uncertainties are divided into three categories: boundary condition, manufacturing and code uncertainties. The boundary condition uncertainties include thermal power, inlet temperature, outlet pressure, and mass flow rate. Uncertainty is also applied to each value in the axial and radial power distribution, after which the distributions are re-normalized so that there isn't an effect on the total thermal power.

The geometry uncertainties are specified as a perturbation of the outer diameter and position of a single corner rod. The values of all boundary condition and geometry uncertainties are shown in Table II. For all parameters with normal distributions, the bounds are defined as three standard deviations.

Table II. Uncertainty parameters from UAM benchmark

Parameter	BWR	PWR	VVER	PDF
Outlet pressure (%)	± 1.0	± 1.0	± 2.0	Normal
Inlet flow rate (%)	± 1.0	± 1.5	± 4.5	Normal
Power (%)	± 1.5	± 1.0	± 0.3	Normal
Inlet fluid temperature (K)	± 1.5	± 1.0	± 2.0	Uniform
Power distribution (%)	± 3.0	± 3.0	± 3.0	Normal
Rod displacement (mm)	± 0.45	± 0.45	± 0.45	Normal
Rod diameter (mm)	± 0.04	± 0.02	± 0.10	Normal

Modeling uncertainties are code-dependent and left to the judgment of the benchmark participants; code uncertainties for this study were determined using expert opinion. The values of modeling uncertainties are shown in Table III. All parameters are assumed to have normal distributions and the bounds are again defined as three standard deviations. The selection of these input uncertainties will be one of the most influential factors in the results of the uncertainty analysis; future work will focus on transitioning from expert opinion to a more quantitative assessment of inherent code uncertainties.

Table III. Modeling uncertainties from expert opinion

Parameter	Accuracy
Single-phase mixing coefficient	± 42 %
Two-phase multiplier for the mixing coefficient	± 24 %
Void drift equilibrium distribution weighing factor	± 14 %
Heat transfer coefficient	± 24 %
Bubbly interfacial drag coefficient	± 32 %
Droplet interfacial drag coefficient	± 26 %
Film interfacial drag coefficient	± 36 %

4. RESULTS AND DISCUSSION

The uncertainty analysis methodology described in the preceding sections was applied to each of the four steady state cases. Using the sample size criterion outlined in Section 2.2, cases 1a, 2a, 2b, 4a, and 5a consisted of 1455, 995, 1075, 1350, and 2720 CTF runs, respectively. For all cases, the skew and kurtosis for each output were used to confirm that the output parameters are approximately normally distributed. The results of the uncertainty analysis are summarized in Table IV and Table V for the BWR and PWR cases, respectively.

Table IV. Global parameter results for BWR cases

	Case 1a			Case 4a		
Parameter	**Nominal**	**Mean**	**St Dev**	**Nominal**	**Mean**	**St Dev**
Maximum Void Fraction	0.738	0.740	0.006 (0.82%)	0.680	0.647	0.010 (1.53%)
Maximum Fuel/Rod Temperature [K]	1928.25	1944.31	22.36 (1.15%)	594.11	594.68	0.71 (0.12%)
Maximum Outside Fuel/Rod Temperature [K]	579.44	579.63	1.01 (0.18%)	561.05	560.90	0.22 (0.04%)
Pressure Drop [kPa]	70.26	70.19	1.21 (1.73%)	70.10	61.16	0.97 (1.59%)

Table V. Global parameter results for PWR cases

	Case 2a			Case 5a		
Parameter	**Nominal**	**Mean**	**St Dev**	**Nominal**	**Mean**	**St Dev**
Maximum Void Fraction	0.001	0.001	0.000	0.340	0.343	0.017 (4.91%)
Maximum Fuel/Rod Temperature [K]	1364.56	1375.64	9.84 (0.72%)	676.57	677.47	0.91 (0.13%)
Maximum Outside Fuel/Rod Temperature [K]	616.81	617.51	0.58 (0.09%)	622.43	642.12	0.83 (0.13%)
Pressure Drop [kPa]	111.00	109.03	0.79 (0.72%)	274.99	274.94	2.55 (0.93%)

The experimental cases (4a and 5a) model cylindrical heated rods, so the maximum rod temperature is at the inside of the cylinder. The nominal values are the results when CTF is run without perturbing any of the input uncertainties; they match well with past benchmarks and studies [9-11]. The resulting uncertainty is very small for all parameters. The nominal and mean value are very similar for most parameters. The exception is the maximum fuel temperature. For Case 1a, the mean and nominal maximum fuel temperature varies by 16 K. The physical location of the maximum fuel temperature in Case 1a can be in four different locations. The behavior of the fuel temperature at each of these locations is different, the mean value is artificially inflated due to the mobility of the global maximum.

Overall sensitivity parameters were found by applying a weighted average to the RCCs. The weight of an entire distribution (i.e. fuel temperature distribution, void fraction distribution, etc.) is equal to the weight of a single global parameter. The results of this averaging scheme are shown in Table VI. These results have no direct physical significance, but are used as a way to rank the most and least important input uncertainty parameters. The inlet temperature is the most important boundary condition uncertainty. The geometry parameters have very small RCCs. The most important modeling uncertainties are the heat transfer coefficient, mixing coefficient and two-phase mixing multiplier.

A number of additional observations can be made from Table VI. The pressure is more important for BWR cases, while the mass flow rate has higher RCCs for the PWR cases. The heat transfer coefficient uncertainty is not important for the single-phase case. Now that the overall sensitivity parameters have been examined, it's also important to compare the individual RCCs.

Table VI. Weighted average results for RCCs

Parameter	1a	2a	4a	5a	Average
Power	0.20	0.18	0.13	0.18	0.17
Pressure	0.22	0.02	0.40	0.01	0.16
Mass Flow Rate	0.07	0.31	0.07	0.22	0.17
Inlet Temperature	0.41	0.59	0.43	0.38	0.45
Geometry	0.03	0.02	0.02	0.02	0.02
Void Distribution Factor	0.01	0.02	0.07	0.02	0.03
Mixing Coefficient	0.12	0.07	0.19	0.22	0.15
Two-Phase Mixing Multiplier	0.06	0.08	0.12	0.14	0.10
Heat Transfer Coefficient	0.26	0.02	0.28	0.48	0.26
Bubbly Drag	0.17	0.02	0.14	0.04	0.09
Droplet Drag	0.02	0.01	0.03	0.02	0.02
Film Drag	0.14	0.01	0.04	0.02	0.05
Axial Power Distribution	0.03	0.04	0.03	0.02	0.03
Radial Power Distribution	0.03	0.03	0.02	0.02	0.03

The RCCs for all of the global parameters for each case are shown in Figure 4. The labels P, $\dot{m}$, Q, T, h, β, Φ, $C_{D,b}$, and $C_{D,f}$ indicate the pressure, mass flow rate, power, inlet temperature, heat transfer coefficient, mixing coefficient, two-phase mixing multiplier, bubbly regime drag coefficient, and film drag coefficient, respectively. The axial and radial labels indicate the locations where the maximum temperature occurs axially and radially.

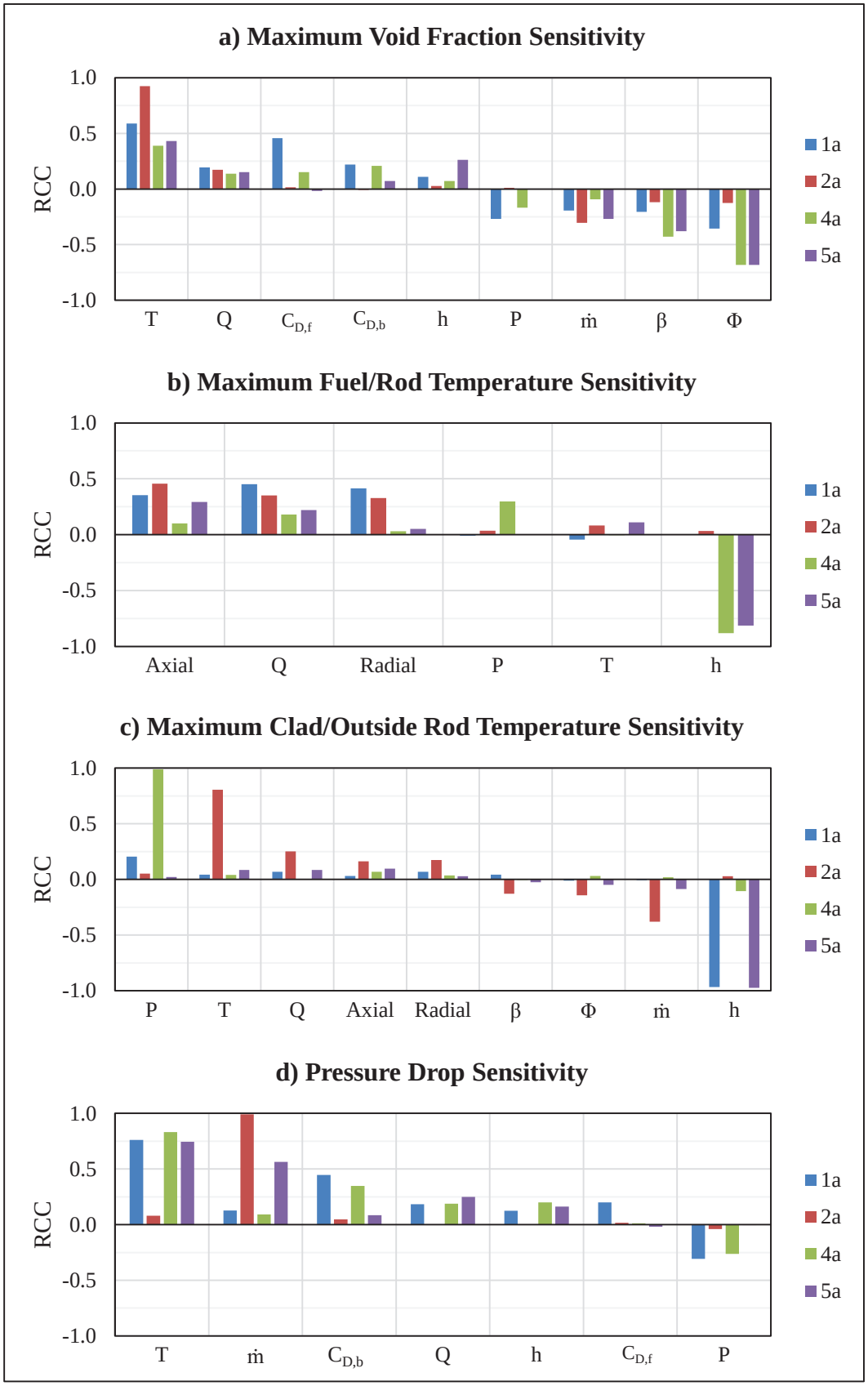

Figure 4. RCCs for the four primary global parameters

The most important parameter for the determination of the maximum void fraction (Figure 4a) is the inlet temperature; the mixing coefficients and bubbly drag coefficient are also influential for cases that have two phases. The film drag coefficient is extremely important for Case 1a, which has the greatest void fraction. The maximum rod temperature (Figure 4b) is heavily influenced by the overall power uncertainty and the value of the power distributions at the locations where the maxima occur.

The maximum cladding or rod outside temperature (Figure 4c) has the most inconsistency in the RCCs, and no obvious trends are observed. The bundle average pressure drop (Figure 4d) is heavily influenced by the inlet temperature for all cases with significant void, the mass flow rate for high pressure cases, and the bubbly drag coefficient for cases with high void fractions.

4.1. Axial Development of Uncertainty/Sensitivity Results

The output parameters include axial distributions of the maximum rod temperature, rod outside temperature, and channel void fraction. It is beneficial to examine these distributions, as it can reveal interesting trends about the development of uncertainty and sensitivity information through a channel. As a demonstration, the void fraction and rod temperature distributions for Case 4a are shown in Figure 5. The red bounds show the minimum and maximum values, as defined by three standard deviations. These distributions are typical for a rod with uniform axial power. The slight dips in the void fraction distribution show the effects of the spacer grids.

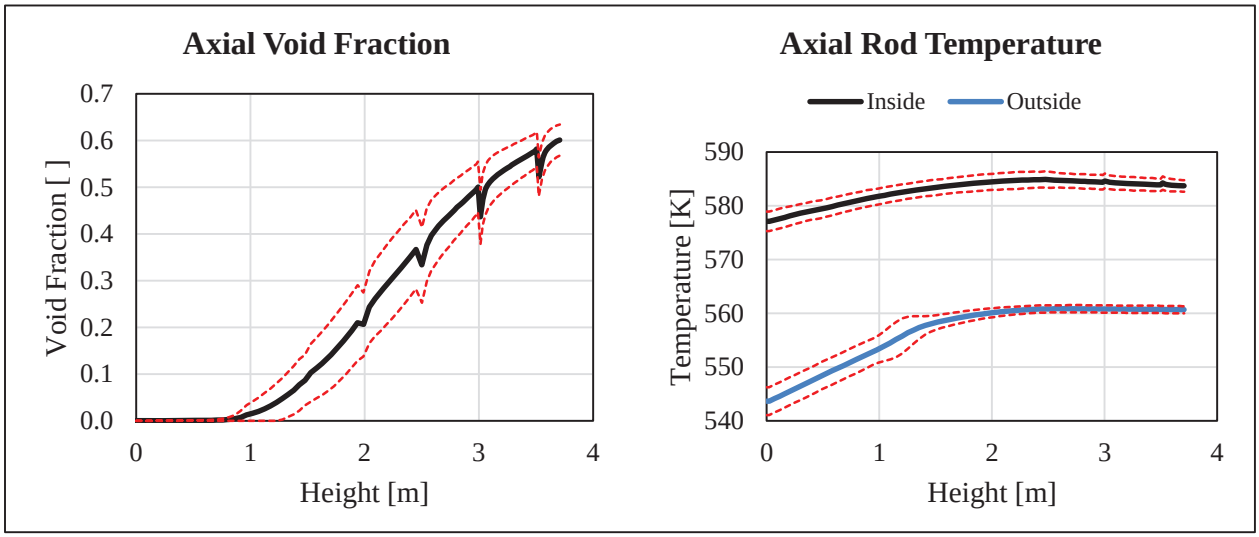

Figure 5. Case 4a axial distribution of void fraction and rod temperatures

The standard deviations are relatively constant over the axial distribution. This is seen across all axial distributions for all four steady state cases.

Additional information can be extracted by examining how the RCCs develop over the axial height. The RCCs of the void fraction for Case 4a are shown in Figure 6. The behavior shown is typical for all four cases. As soon as void is present, the inlet temperature RCC increases immediately. The heat transfer coefficient RCC slightly increases and decreases. The mixing coefficient and power have slightly positive RCCs and the pressure RCC is slightly negative. The effect of the grid spacers on the heat transfer and mixing coefficients can be seen in their respective RCCs, because the heat transfer and mixing enhancement models in CTF were not accounted for in this uncertainty analysis.

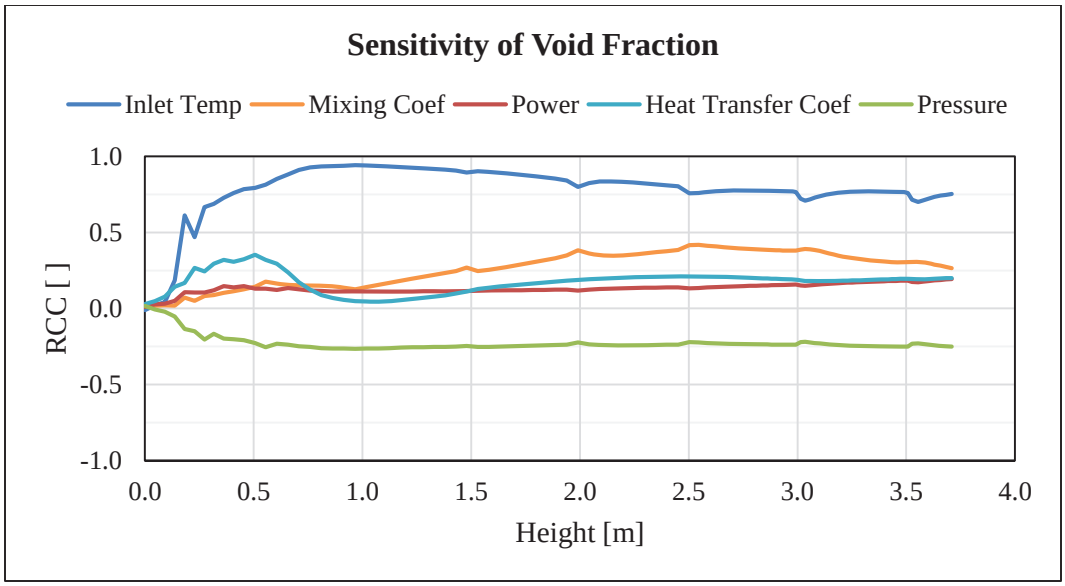

Figure 6. Case 4a axial development of RCCs for void fraction

The development of the rod outside temperature RCCs over the axial length are shown in Figure 7. This behavior is very interesting, as the inlet temperature and exit pressure exchange their RCC values through the axial height of the channel. This is because both parameters are applied as boundary conditions at the inlet and outlet, so they will strongly influence the temperature in their respective regions.

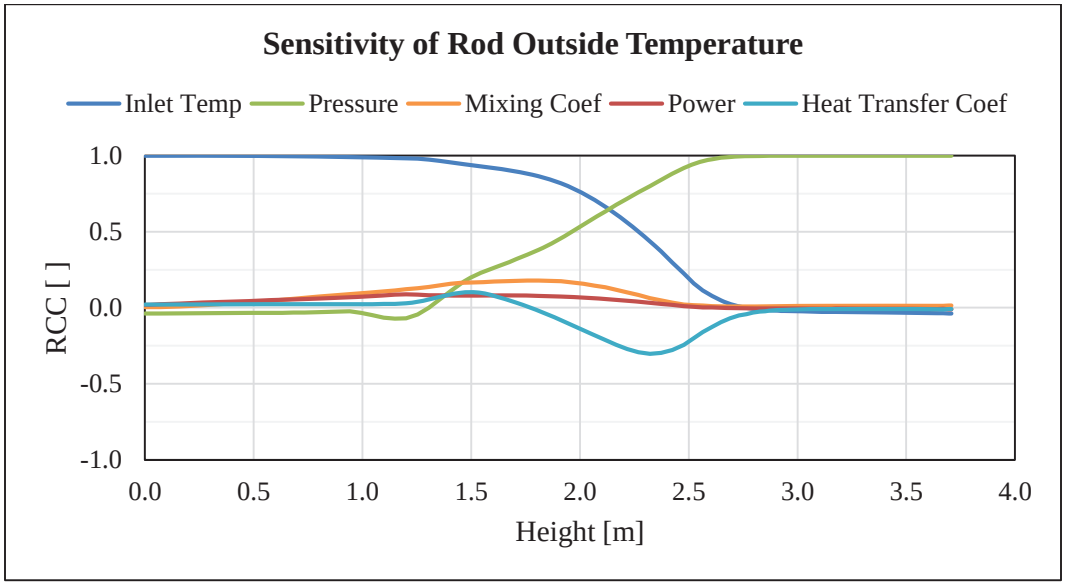

Figure 7. Case 4a axial development of RCCs for outside rod temperature

The centerline temperature sensitivities behave in a similar manner, except that they are less smooth, the power RCC is higher, and the pressure is less important. Also, each point in the axial power distribution is very important in the vicinity of where it is applied. The PWR cases have very similar behavior, but the

pressure uncertainty is less important. For the single phase case, the RCCs are relatively constant over the axial height.

4.2. Transient Development of Uncertainty/Sensitivity Results

An uncertainty and sensitivity analysis was also performed on Case 2b, the TMI transient. The relative variation of the boundary conditions was shown in Figure 3. Using these values, the uncertainty in the global parameters (maximum void fraction and temperatures, pressure drop) was found over the five second transient. The most interesting of these results for a flow reduction transient is the bundle average pressure drop, which is shown in Figure 8.

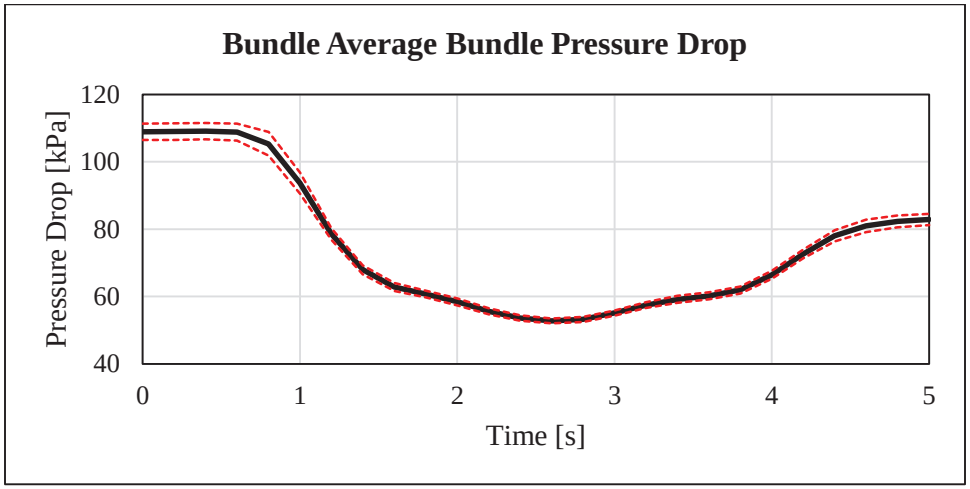

Figure 8. Case 2b bundle average pressure drop

For all parameters, the relative uncertainty is approximately constant over the length of the transient; this result is shown in Figure 9. One would expect the uncertainty from earlier time steps to propagate through the transient to later time steps. This is due to the method for implementing the boundary condition uncertainties throughout the transient.

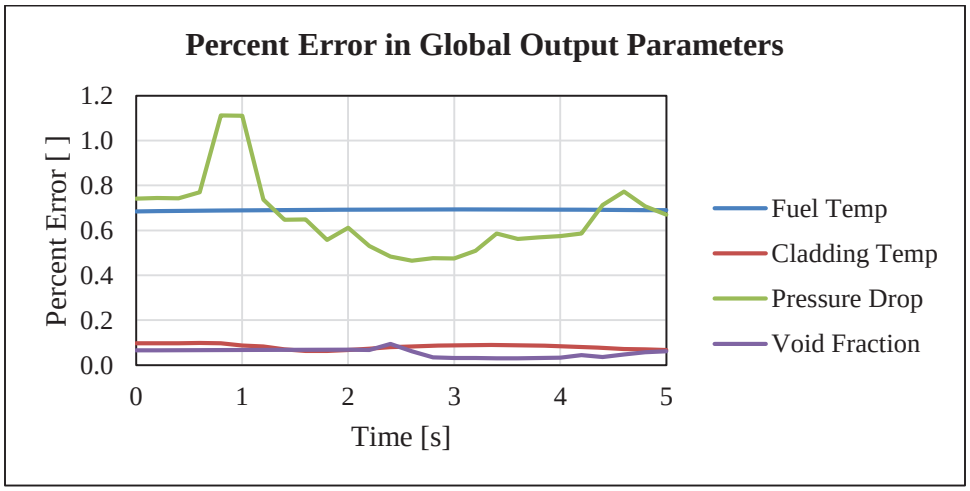

Figure 9. Case 2b change in percent error over time

The boundary condition uncertainties were only applied to the initial conditions, and then the transient values are input relative to the initial value. This method is not specified in the UAM benchmark, and more physical results could be achieved by applying a separate uncertainty at each time step. Applying individual uncertainties at each time step would result in an unrealistically large number of input uncertainties, so this method was not used. All of the RCCs during the transient are approximately constant with time, except for the inlet temperature and pressure boundary conditions.

4.3. Treatment of Geometry Uncertainties

The UAM specification suggests accounting for manufacturing uncertainties by perturbing the location and outer diameter of a single corner rod. Past results for the benchmark have suggested that this geometry treatment has an extremely small contribution to the overall uncertainty of the output parameters. If the perturbation of all rods simultaneously has little influence on the output parameters, then the neglect of geometry uncertainties is a valid approach for future work.

To confirm this hypothesis, an algorithm was designed to perturb the geometry of all rods in Case 1a and 5a. The rod displacement distribution, outer diameter distribution, and a uniformly distributed angle were used to perturb each rod and then calculate changes in the flow area and wetted perimeter for each of the surrounding subchannels. The average percent difference between the means and standard deviations for all output parameters with and without geometry perturbations for all rods are shown in Table VII.

Table VII. Average percent difference between statistical parameters when accounting for all geometry perturbations

	Case 1a	Case 5a
Mean Value	0.06%	0.08%
Standard Dev	1.72%	1.48%

In addition to these very small changes in the overall uncertainty results, the RRCs for the rod diameters, displacements, and angles were low for both cases. As such, the contribution of geometry uncertainties has been shown to be negligibly small; the treatment of geometry uncertainties in CTF is a trivial exercise.

5. CONCLUSIONS

A thorough uncertainty and sensitivity analysis was conducted for four steady state cases and one transient case from the UAM benchmark. Uncertainty results for the maximum void fraction, maximum centerline temperature, maximum outside rod temperature, and bundle average pressure drop were reported. The development of uncertainty and sensitivity data over axial height was discussed. The results for the transient case revealed a possible error in the methodology implied by the UAM benchmark, but additional work will be required to confirm. The five major conclusions from this study are as follows:

1. The boundary condition uncertainties are all important, with the inlet temperature providing the largest contribution.
2. The only modeling parameters from this study that contributed significantly to the output uncertainties were the heat transfer coefficient, the bubbly and film drag coefficients and the mixing coefficients.

3. The axial and radial power distributions are not important to the overall simulation, but they heavily influence the rod temperatures in their vicinities.
4. Much of the uncertainty and sensitivity data is heavily dependent on the presence of the second phase. Uncertainties are generally larger for cases with significant void, and the RCCs are approximately constant over the axial height for the case with only one phase. In addition, the heat transfer coefficient uncertainty is more important for high void fractions.
5. Geometry uncertainties should be neglected in future CTF uncertainty analyses.

Higher fidelity uncertainty analyses of CTF can be achieved through a quantitative method for the determination of the modeling parameter uncertainties. Future work will achieve this by identifying important correlations with sensitivity studies, exposing correlation coefficients, and applying parameter distributions that have been reconstructed using Bayesian calibration methods. These distributions can be used to give better estimates of the input modeling uncertainties inherent in CTF. The scope of this thorough analysis is very large, so initial sensitivity analyses will be very important to focus the work on the most influential uncertainties.

6. REFERENCES

1. T. Blyth, et al., "Benchmark for Uncertainty Analysis in Modeling (UAM) for Design, Operation and Safety Analysis of LWRS, Volume II: Specification and Support Data for Core Cases," *OECD NEA/NSC/DOC* (2014).
2. R. Salko and M. Avramova, "CTF Theory Manual," PSU RDFMG (Nov 2014).
3. B. Adams, et al., "Dakota Version 6.0 Theory Manual," *Sandia National Laboratories*, Albuquerque (2014).
4. "COBRA-TF," www.casl.gov/COBRA-TF.shtml.
5. B. Adams, et al., "User Guidelines and Best Practices for CASL VUQ Analysis Using Dakota," *CASL* (2014).
6. S. S. Wilks, "Determination of Sample Sizes for Setting Tolerance Limits," *The Annals of Mathematical Statistics*, **12**(1), pp. 91-96 (1941).
7. B. Neykov, et al., "OECD-NEA/US-NRC/NUPEC BWR Full-size Fine-mesh Bundle Test (BFBT) Benchmark," *OECD NEA/NSC/DOC* (2005).
8. A. Rubin, et al., "OECD/NRC Benchmark Based on NUPEC PWR Subchannel and Bundle Tests (PSBT)," *NEA/NSC/DOC* (2010).
9. Y. Perin, et al., "Uncertainty Analysis of CTF Prediction of Moderator and Fuel Parameters for the OECD LWR UAM Benchmark using, Exercise II-3," *Proceedings of NURETH-15*, Pisa, Italy, May 12-15 (2013).
10. M. Avramova, et al., "Analysis of Steady State and Transient Void Distribution Predictions for Phase I of the OECD/NRC BFBT Benchmark using CTF/NEM," *Proceedings of NURETH-12*, Pittsburgh, USA, Oct (2007).
11. M. Avramova, et al., "Comparative analysis of CTF and TRACE Thermal-Hydraulic Codes using OECD/NRC PSBT Benchmark Void Distribution Databate," *Proceedings of NURETH-14*, Toronto, Canada, Sept 25-29 (2011).